Highland contamination in lunar mare soils: Improved mapping with multiple end-member spectral mixture analysis (MESMA)

Lin Li[1] and John F. Mustard

Department of Geological Sciences, Brown University, Providence, Rhode Island, USA

Received 15 April 2002; revised 3 February 2003; accepted 21 February 2003; published 14 June 2003.

[1] Multiple end-member spectral mixture analysis (MESMA) was applied to the Clementine UVVIS global 1 km multispectral data set, and the resulting highland material fraction image was used to investigate highland contamination of mare surfaces by impact cratering. MESMA decomposes each pixel with the number of end-members fewer than the number of the spectral bands of Clementine UVVIS data. This allows the use of variable end-member combinations to accommodate global spectral variance. A 13-end-member set of lunar soil components that spans the lunar spectral diversity was selected from the UVVIS data and included 1 mature and 4 fresh highland soils, 4 mature and 2 fresh mare soils, and 2 soils of dark mantling materials. This set was applied to the lunar data through MESMA, and an aggregated global highland abundance was derived. Comparison of the highland fraction results from MESMA and traditional spectral mixture analysis (SMA) demonstrated that MESMA better accommodates the compositional variation of mare soils, resulting in a greater accuracy in the measurement of highland. With the derived products, we investigated highland contamination in Mare Nectaris, Mare Fecunditatis, and Mare Crisium. These mare surfaces are proximal to the large craters Theophilus, Taruntius, Langrenus, and Proclus and provided an opportunity to investigate highland contamination by large impacts. The analyses indicated that Theophilus impact resulted in highland contamination of 20–80% on most of Mare Nectaris, while Taruntius and Langrenus impacts caused 5–40% contamination of Mare Fecunditatis. The trend of minimal highland abundance in Mare Fecunditatis correlates poorly with basalt thickness, suggesting an efficient lateral mixing due to the large craters Taruntius and Langrenus. Additionally, Proclus, combining with other craters, was responsible for highland contamination in most of the Mare Crisium surface, and some basalt classification in this mare reflects highland contamination of the spectral properties. MESMA significantly reduces uncertainty in calculating global composition variations due to mixing, and these analyses demonstrate that large impacts played a dominant role in delivering highland materials onto three mare surfaces. *INDEX TERMS:* 5470 Planetology: Solid Surface Planets: Surface materials and properties; 5464 Planetology: Solid Surface Planets: Remote sensing; 5420 Planetology: Solid Surface Planets: Impact phenomena (includes cratering); 5139 Physical Properties of Rocks: Transport properties; *KEYWORDS:* Highland contamination, mare soils, lateral mixing, Moon

Citation: Li, L., and J. F. Mustard, Highland contamination in lunar mare soils: Improved mapping with multiple end-member spectral mixture analysis (MESMA), *J. Geophys. Res.*, *108*(E6), 5053, doi:10.1029/2002JE001917, 2003.

1. Introduction

[2] Since the discovery of highland components in mare soils returned by the Apollo missions, there has been a vigorous debate among lunar scientists regarding their provenance [*Florenskiy et al.*, 1974; *Gault et al.*, 1974; *Rhodes*, 1977; *Hörz*, 1978]. Some propose that the exotic components come from remote highland regions through lateral transport. Others suggest that these components originate from the highland material beneath the mare by vertical mixing [*Quaide and Oberbeck*, 1975; *Rhodes*, 1977; *Hörz*, 1978]. This distinction between lateral and vertical mixing has important implications for understanding the provenance of lunar rocks and soils and crater ejecta emplacement, and needs to be included in planning for future sample return missions. It also raises a question of how representative lunar soil samples are of the bedrock composition.

[3] To support the lateral transport concept, it is necessary to demonstrate there has been the movement of highland

[1]Now at Center for Spatial Technologies and Remote Sensing, Department of Land, Air and Water Resources, University of California, Davis, California, USA.

0148-0227/03/2002JE001917$09.00

components, constituting 10–20% of mare soils, to sites tens to hundreds of kilometers from the nearest source [*Hörz*, 1978; *Hörz et al.*, 1991]. Estimates of the amount of exotic component contents within large-scale compositional gradients supports the concept of materials have been dispersed from a specific source. In previous studies, we investigated lunar surface mixing by applying spectral mixture analysis (SMA) to Clementine UVVIS data [*Mustard et al.*, 1998; *Li and Mustard*, 2000]. These studies focused on lateral transport of lunar materials across mare-highland boundaries due to many small craters. Large craters were not included. *Oberbeck et al.* [1975] and others have addressed the mixing of ejecta from large craters with local materials through theoretical models [*Oberbeck et al.*, 1974, 1975; *Schultz and Gault*, 1983, 1985]. However, little research exists using remote sensing observations to quantify the compositional gradients formed by lateral transport due to large craters [*Li and Mustard*, 2001]. *Pieters et al.* [1985] observed the material mixing processes along rays extending from the crater Copernicus, but observed highland and mare mixing was evidently due to vertical mixing. In this study, we address two fundamental issues of lateral transport related to large craters: (1) whether large craters are responsible for the highland content in mare soils; and (2) if so, how much highland contamination exists in mare soils.

[4] Traditional SMA is ill-suited to calculating the global distribution of lunar surface components. The maximum number of components that SMA can map is limited by the number of bands in the image data. In relatively small regions with only a few geological components, SMA can be used to map the compositional distribution with reasonable accuracy [*Mustard et al.*, 1998; *Li and Mustard*, 2000]. However over large regions extending to global scales, the number of the lunar surface components far exceeds the number of bands in Clementine UVVIS data, eliminating the application of traditional SMA.

[5] Multiple end-member SMA (MESMA) [*Roberts et al.*, 1998] overcomes the limitations of traditional SMA. MESMA assumes that although an image contains a large number of spectrally distinct components, individual pixels contain a limited subset of these whose number is fewer than the number of bands. The method decomposes each pixel using different combinations of possible end-members, allowing a large number of end-members to be utilized across a scene. With a restricted end-member data set, MESMA starts with all possible two end-member combinations for a pixel and determines the optimal mixture model on the basis of two criteria: physically reasonable fractions and lower RMS error. If a two-end-member model fails to fit a pixel spectrum, then a three end-member model is constructed according to similar criteria, and so on.

[6] In the next section, we briefly describe the data used and our methods. The identified Clementine end-members of lunar soils are presented in section 3. The results of MESMA are presented in section 4, where differences in results from SMA and MESMA are discussed. In section 5, we investigate highland fractions in Mare Nectaris, Mare Fecunditatis, and Mare Crisium with MESMA generated maps. These mare surfaces are selected because of their proximity to the large craters of Theophilus, Taruntius, Langrenus, and Proclus, and thus provide an opportunity to investigate highland contamination by large impacts.

2. Data and Methods

2.1. Data Description and Preprocessing

[7] The data used in this study are the Clementine UVVIS (ultraviolet-visible) global mosaic image created by the U. S. Geological Survey [*Robinson et al.*, 1999; *Eliason et al.*, 1999; *Isbell et al.*, 1999]. These data consist of five spectra bands with wavelengths centered at 0.45, 0.75, 0.90, 0.95 and 1.0 μm. The high-resolution, nominal 100 m, raw Clementine UVVIS data were calibrated, mosaicked, and lastly degraded to one-kilometer resolution.

[8] The calibration provided radiometric and photometric normalization including corrections for electronic gain and offset, dark-current, signal gain during the frame transfer, nonlinearity and temperature offset, nonuniformity of sensitivity across the detector, and exposure time. The data were also normalized to the Earth-Sun (1-AU) distance and converted to corresponding radiance. The data were finally converted into reflectance and normalized to the standard angle geometry: phase = 30°, emergence = 0°, and incidence = 30° [*McEwen et al.*, 1998; *Eliason et al.*, 1999; *Gaddis et al.*, 2000].

[9] Since lunar soils are intimately mixed on the Moon, nonlinear mixing is expected [*Pieters et al.*, 1985; *Mustard et al.*, 1998]. We thus employed a nonlinear spectral mixing procedure based on *Hapke*'s [1981] model to unmix the data [*Mustard and Pieters*, 1989]. The reflectance data were first converted to single scattering albedo (SSA) using a simple look-up table generated with (1):

$$R(i,e,g) = \frac{w}{4(\mu+\mu_0)} H(\mu)H(\mu_0), \tag{1}$$

where $\mu = \cos(i)$, $\mu_0 = \cos(e)$, i is the incidence angle; e is the emergence angle; g is the phase angle; w is the single scattering albedo; and $H(\mu) = (1+2\mu)/\left(1+2\mu\sqrt{1-w}\right)$ which describes multiple scattering between particles [*Hapke*, 1993]. This simplified form follows *Mustard and Pieters* [1987] and is appropriate for the viewing geometry of the normalized Clementine UVVIS data assuming isotropic scattering and no opposition effect. Intrinsic problems of nonlinear mixtures can thus be linearized by converting reflectance into single scattering albedo. After the conversion, the end-member fractions are readily calculated from a group of linear equations by using a least squares method [*Mustard and Pieters*, 1989].

2.2. Multiple End-Member Spectral Mixture Analysis

[10] With the 13 end-members described in section 3, we decomposed each pixel with all possible two end-member combinations and evaluated the results using two criteria: physically plausible fractions and the lowest RMS error. In theory, physically plausible fractions range from 0 to 1.0, but a range from −0.05 to 1.05 is used here to accommodate the effect of measurement error and noise. In the same way, three end-member models can be constructed and evaluated. However, there will always be a three-end-member model that results in a lower RMS than

a 2-end-member model, but the three-end-member model may overfit the data. We used an estimated data noise level to select the appropriate model. If a two-end-member model produced an RMS error less than the noise level, this model was used and no three-end-member models were calculated. Otherwise, the optimum 3-end-member model was used. For the thirteen-end-member data set, 78 two-end-member models were run for each pixel and for those pixels that required it, 286 three-end-member models were run.

2.3. Identification of Mixture Model End-Members

[11] Our approach to identifying an optimal end-member set is based on spectral interpretation of lunar soils and guided by our knowledge of lunar surface processes. The key spectral features of lunar materials in the wavelength range of the Clementine UVVIS data included albedo, UVVIS slope from 0.415 to 0.75 μm and an absorption feature between 0.90 and 1.0 μm. The absorption minima are largely due to mafic minerals (e.g., pyroxene), while variations in the slope arise from several factors. Lunar materials are broadly divided into three categories: highland, mare and fresh crater materials. Mature highland soils have a high albedo due to abundant plagioclase, a relatively steep UVVIS slope, and exhibit a very weak iron absorption feature at or near 1.0 μm. Mare soils are largely composed of iron-bearing minerals resulting in a lower albedo and stronger 1.0 μm band absorption. The variation in the UVVIS slope of mare soil spectra is related to TiO_2 content [*Charette et al.*, 1974; *Pieters*, 1978]. Fresh crater materials are brighter in albedo and show a stronger absorption feature near 1.0 μm relative to the equivalent mature soils. Fresh highland crater material has the highest albedo on the lunar surface [*Pieters et al.*, 1993].

[12] Band ratios are frequently used to describe the UVVIS slope and absorption strength [*Pieters et al.*, 1994; *Weitz et al.*, 1998; *Yingst and Head*, 1999; *Gaddis et al.*, 2000]. We therefore use 0.415 to 0.75 μm and 0.95 to 0.75 μm reflectance ratios as an aid in end-member identification. A high 0.415/0.75 band ratio indicates high Ti content in mare basalt. A low 0.95/0.75 ratio implies a strong mafic absorption band.

[13] In addition, we also applied the techniques of *Lucey et al.* [1998, 2000a, 2000b] to estimate FeO and TiO_2 content and refine the end-member set. Estimating FeO and TiO_2 required an optimal coordinate origin. For estimating FeO content, the optimal reflectance minimum found was 0.08 for the 0.75 μm reflectance, and an optimal value of 1.19 for the 0.95/0.75 μm ratio. For estimating TiO_2 content, the 0.75 μm reflectance minimum was 0.0 and the 0.415 μm/0.75 μm optimized value was 0.42 [*Lucey et al.*, 2000a].

[14] The ratios 0.415 μm/0.75 μm and 0.95 μm/0.75 μm are not only sensitive to the chemical compositions, but also to the maturity of materials. To distinguishing fresh from mature materials, we applied an algorithm after *Lucey et al.* [2000b] to isolate the effects of maturity on the interpretation of composition and end-member selection.

[15] The algorithms for mapping FeO, TiO_2 and maturity were not used to identify the dark mantling materials because the effects of pyroclastic glasses on the algorithms are not clearly understood due to the variation in the optical behavior of pyroclastic glasses [*Johnson et al.*, 1991; *Lucey et al.*, 1998].

Table 1. End-Member Locations and Derived FeO and TiO_2 and Maturity for Each of Them

EM Code	Latitude	Longitude	%FeO	%TiO_2	Maturity
MM1	2°27′25.42″S	43°8′13.74″W	20.1	16.8	0.16
MM2	58°13′34.10″N	16°13′34.63″W	14.9	0.4	0.21
MM3	20°47′37.82″N	56°43′28.19″W	19.2	11.5	0.18
MM4	16°36′19.37″N	62°51′28.71″E	18.8	8.0	0.15
DK1	10°14′24.86″N	5°20′33.35″E	-[a]	-[a]	-[a]
DK2	26°47′46.32″N	52°26′14.02″W	-[a]	-[a]	-[a]
FM1	29°59′42.94″N	24°53′56.92″E	16.1	2.4	0.48
FM2	59°18′52.13″N	13°49′7.75″W	15.8	0.5	0.46
MH	49°11′22.63″N	130°49′39.69″E	1.7	0.2	0.15
FH1	64°47′20.98″N	29°32′57.06″E	1.4	0.0	0.39
FH2	43°13′13.22″S	11°18′44.69″W	7.5	0.1	0.48
FH3	57°45′51.91″N	24°30′12.23″E	5.0	0.1	0.44
FH4	13°12′30.74″S	94°23′11.46″W	2.5	0.1	0.47
FM	27°45′9.43″N	11°46′24.61″E	16.2	2.5	0.36
FH	23°39′47.16″N	47°15′34.29″W	2.9	1.1	0.38
HSMA	35°34′7.97″N	92°10′36″W	2.8	0.3	0.13

[a]The algorithms are not applicable.

3. Lunar Soil End-Members

[16] Geographic coordinates of end-members and derived parameters FeO and TiO_2 and maturity used for distinguishing them are listed in Table 1. The plots of 0.75 μm versus 0.415/0.75 μm ratio in Figure 1a, and the 0.95/0.75 μm ratio versus 0.415/0.75 μm ratio in Figure 1b demonstrate the distinctiveness of 13 end-members used by MESMA. A 3-D plot of the derived parameters FeO, TiO_2 and maturity is shown in Figure 2.

3.1. Mature Mare Basalt

[17] The TiO_2 abundance of mare basalts varies widely, and has been empirically tied to the spectral properties of albedo and UVVIS ratio through a number of approaches [*Charette et al.*, 1974; *Pieters and McCord*, 1976; *Johnson et al.*, 1977, 1991; *Melendrez et al.*, 1994; *Giguere et al.*, 2000]. The range of TiO_2 content in mare basalts is generally classified into high, medium high, medium, and very low. A TiO_2 map was used to distinguish mare end-members. We also selected areas of relatively pure mare by referring to the FeO map. The end-members were selected in areas of high FeO content because the presence of highland in mare soils would dilute FeO content of the soils. Four mature mare end-members were selected (Figure 2).

3.1.1. Mature Mare End-Member 1 (MM1)

[18] This end-member was selected in the Flamsteed region, where mare basalt filled the large, 112 km diameter, crater Flamsteed P [*Pieters et al.*, 1980]. High TiO_2 content controls the albedo, spectral contrast and the UVVIS ratio of this mare basalt [*Pieters*, 1978]. The shallowest UVVIS slope, the lowest overall albedo and the weakest band absorption features make MM1 distinguishable spectrally from other end-members. MM1 represents FeO and TiO_2 values of 20.13% and 16.82%.

3.1.2. Mature Mare End-Member 2 (MM2)

[19] MM2 was extracted from Eastern Frigoris where very low-Ti mare basalt is dominant [*Pieters*, 1978; *Wilhelms*, 1987]. MM2 exhibits the highest overall albedo, and the steepest UVVIS slope among all selected mare end-

members due to the low TiO_2 contents (0.4%). A strong absorption feature at 1.0 μm was interpreted as the effect of the Fe-rich homogenous glass or pyroxene, and the soil has approximately 15% FeO.

3.1.3. Mature Mare End-Members 3 and 4 (MM3 and MM4)

[20] MM3 was selected in a mare region dominated by medium high-Ti basalt, just southwest of the Aristarchus Plateau. MM4 was located in Crisium mare. Both MM3 and MM4 had UVVIS ratios and albedo ranging between MM1and MM2. Although MM3 and MM4 had similar UVVIS slopes, MM3 exhibited lower overall albedo because of higher Ti content than MM4. Estimated contents for MM3 were 11.5% TiO_2 and 19.16% FeO, and for MM4, 8% TiO_2 and 18.8% FeO.

3.2. Mature Highland

3.2.1. Mature Highland End-Member (MH)

[21] This end-member was extracted from the image after referring to a maturity map to avoid fresh highland materials, and from a region with relatively smooth topography to avoid the influence of illumination geometry. This example end-member was estimated to contain 1.65% FeO and 0.18% TiO_2. However, keep in mind that the compositional variation of highland materials is very broad due to the systematic differences among highland soils [*Pieters et al.*, 1993]. For example, the high albedo of highland soil was probably associated with significant amount of Al-rich plagioclase [*Pieters et al.*, 1993; *Tompkins and Pieters*, 1999].

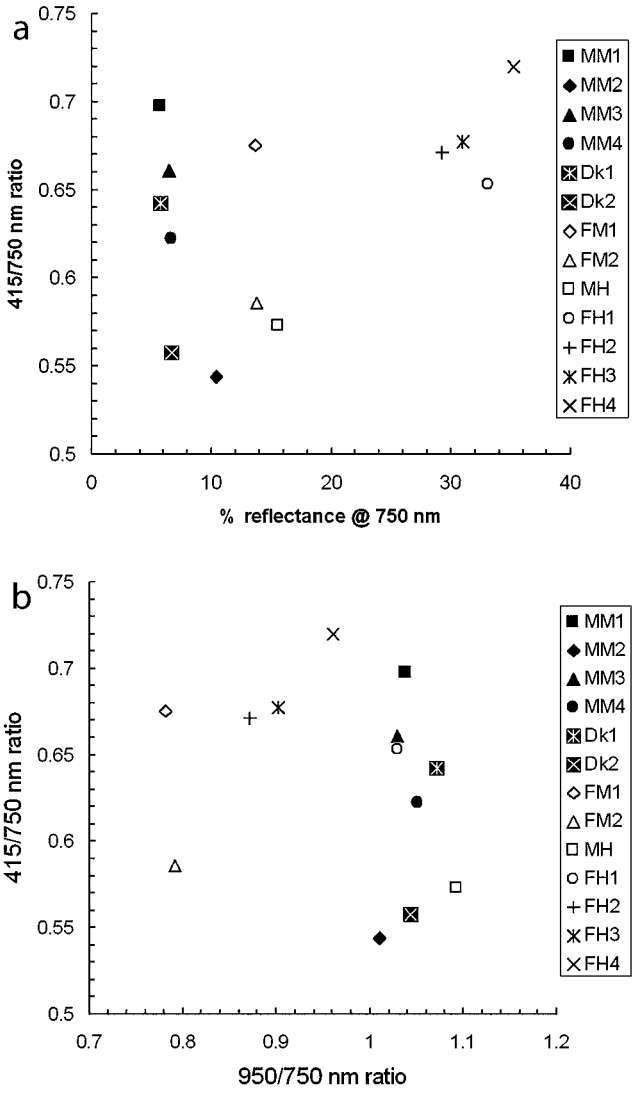

Figure 1. Spectral parameter plot for 13 end-members used by MESMA, (a) 0.75 μm versus the 0.415/0.75 μm ratio, (b) the 0.95/0.75 μm versus the 0.415/0.75 μm ratio.

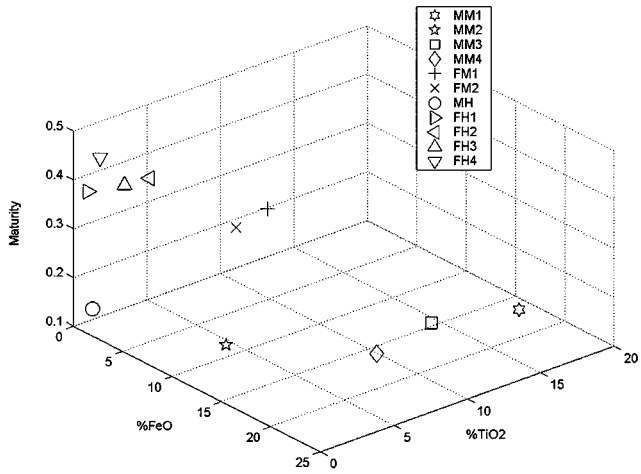

Figure 2. A 3-D plot of derived parameters FeO, TiO_2 and maturity shows the distinctiveness of end-members used by MESMA. End-members of dark mantling materials are not included.

3.3. Fresh Mare Craters

[22] Fresh mare craters are readily distinguished from mature mare soil by their relatively high albedo and exhibit a strong absorption feature near 1.0 μm due to pyroxene. Two end-members were selected for this study.

3.3.1. Fresh Mare End-Member 1 (FM1)

[23] FM1 was extracted from a mare crater in Serenitatis and exhibits a strong absorption band near 1.0 μm. It represents fresh material from medium-Ti mare basalt.

3.3.2. Fresh Mare End-Member 2 (FM2)

[24] FM2 was located in Mare Frigoris, representing low-Ti mare and has the absorption feature at 1.0 μm.

3.4. Fresh Highland Craters

[25] Fresh highland craters are the best analogue on the Moon to crystalline rock powders exhibiting diagnostic mineral absorption features. The diagnostic features were linked to the types and abundance of mafic minerals [*Pieters*, 1977]. *Stöffler et al.* [1980] classified highland rock into anorthosite (>90% plagioclase) and mafic-bearing rock types. The mafic-bearing rock types are composed of plagioclase with various amounts of pyroxenes and olivine [*Stöffler et al.*, 1980]. On the basis of the Stöffler et al. classification scheme, *Tompkins and Pieters* [1999] proposed a simplified Clementine classification scheme. We used *Tompkins and Pieters* [1999] classification to extract four end-members of fresh highland materials, representing anorthosite, gabbro, norite and olivine-rich material.

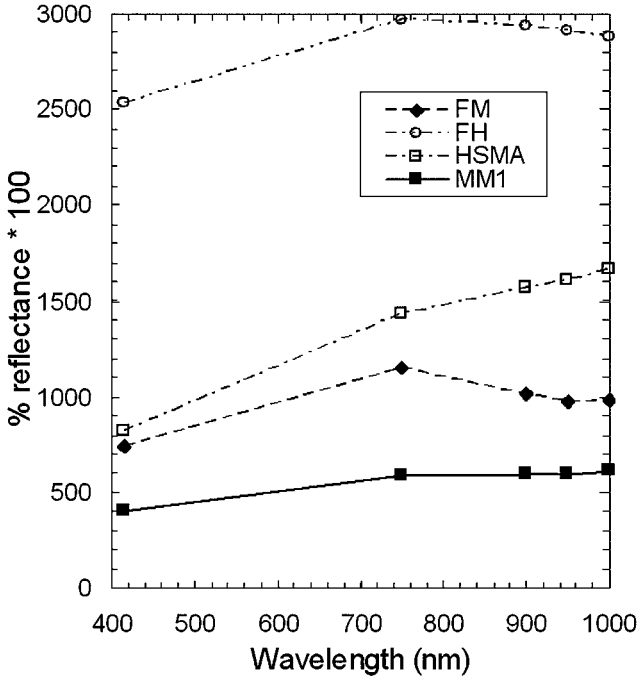

Figure 3. Reflectance spectra of end-members for traditional SMA, representing mature mare (MM), fresh mare (FM), mature highland (HSMA) and fresh highland (FH).

3.4.1. Fresh Highland End-Member 1 (FH1)

[26] This end-member is anorthositic with a high amount of plagioclase (>90%) and lacking mafic minerals (<1%). It has the highest bulk albedo among all end-members, and very low concentration of FeO.

3.4.2. Fresh Highland End-Member 2 (FH2)

[27] This gabbroic end-member exhibits a strong absorption feature at 0.95 μm indicating that high-Ca pyroxene is the primary mafic mineral.

3.4.3. Fresh Highland End-Member 3 (FH3)

[28] This end-member is noritic and contains low-Ca pyroxene as a dominant mafic mineral, identifiable by a strong 0.90 μm absorption feature.

3.4.4. Fresh Highland End-Member 4 (FH4)

[29] Since the presence of olivine is often masked spectrally by pyroxene, it is difficult to distinguish olivine from pyroxene. However, with the spectral range and resolution of Clementine data, it is possible to make the distinction between lithologies that are dominated by pyroxene and those by olivine [*Pieters et al.*, 1997, 2001; *Tompkins and Pieters*, 1999]. We chose to separate gabbroic rock (FH2) and norite (FH3) from olivine-rich material (FH4) by a single downward inflection at the three near infrared bands, 0.90, 0.95 and 1.0 μm. This downward inflection is diagnostic of the presence of olivine because it has a much broader absorption centered at a longer wavelength than pyroxene. Lithologies dominated by pyroxene would exhibit a concave spectrum through 0.90, 0.95 and 1.0 μm [*Pieters and Tompkins*, 1999].

3.5. Dark Mantled Surface

[30] Dark mantling material has been identified using a variety of remote sensing observations at both regional and local scales [e.g., *Head*, 1974; *Gaddis et al.*, 1985, 2000; *Weitz et al.*, 1998]. The material had a low albedo and fine texture in remotely sensed data due to the abundant fine grained glasses [*Zisk et al.*, 1977].

[31] We defined two end-members to represent pyroclastic deposits (Figure 2) from dark mantling deposits.

3.5.1. Dark Mantling Material 1 (DK1)

[32] DK1, in Mare Vaporum, had a high 0.415/0.75 ratio, indicating a Ti-rich unit and a high 0.95/0.75 ratio indicating crystallized Fe-Ti glass of opaque ilmenite-rich spheres [*Pieters et al.*, 1993]. DK1 is similar to the "black bead" glass of Apollo 17, sample 74001.

3.5.2. Dark Mantling Material 2 (DK2)

[33] DK2 is spectrally similar to the homogeneous orange glass of Apollo 17, sample 74220. This site has a steep UVVIS slope and a strong 1 μm feature due to Fe-bearing glasses [*Pieters et al.*, 1993; *Greeley et al.*, 1993; *Weitz et al.*, 1998].

3.6. End-Members for Traditional Spectral Mixture Analysis

[34] The traditional spectral mixture analysis was also conducted to compare with MESMA results. The four end-members representing mature high-Ti mare, mature highland, and spectrally fresh highland and mare crater materials are used. They are assigned to the numbers 1, 14, 15, and 16 in Table 1, and labeled as MM1, HSMA, FH and FM. The reflectance spectra of the four end-members are shown in Figure 3.

4. Results and Discussions

4.1. MESMA Results

[35] Application of the MESMA resulted in thirteen data layers representing the global abundance of each end-member at a 1 km resolution. To focus on the mixing between mare and highland components, we grouped 12 of the 13 fraction images into four by adding relevant fraction images together. In this way, the two fraction images for fresh mare craters were consolidated into one. The similar operations were applied to two dark mantling material and the four mature mare fraction images. The operation also aggregated four fresh highlands into one image. Mature highland has one end-member only and the aggregation is not necessary.

[36] The fraction images of the fresh highland and mare were related to the maturity of the lunar surface. To focus on the relative proportion between highland and mare materials independent of optical maturity, we used equation (7) of *Li and Mustard* [2000] to normalize the mare fraction image:

$$F_{m\_norm} = \frac{F_m}{F_m + F_h}, \tag{2}$$

where F_m and F_h are the mare and highland abundance, and F_{m_norm} is the normalized abundance within each pixel.

4.2. MESMA Versus Traditional SMA

[37] We suspected that the SMA abundance estimates were biased by the TiO_2 variation among mare regions. To demonstrate this bias, we compare the results of MESMA and SMA in two different regions with well-defined compositional boundaries: (1) between Mare Serenitatis and Mare

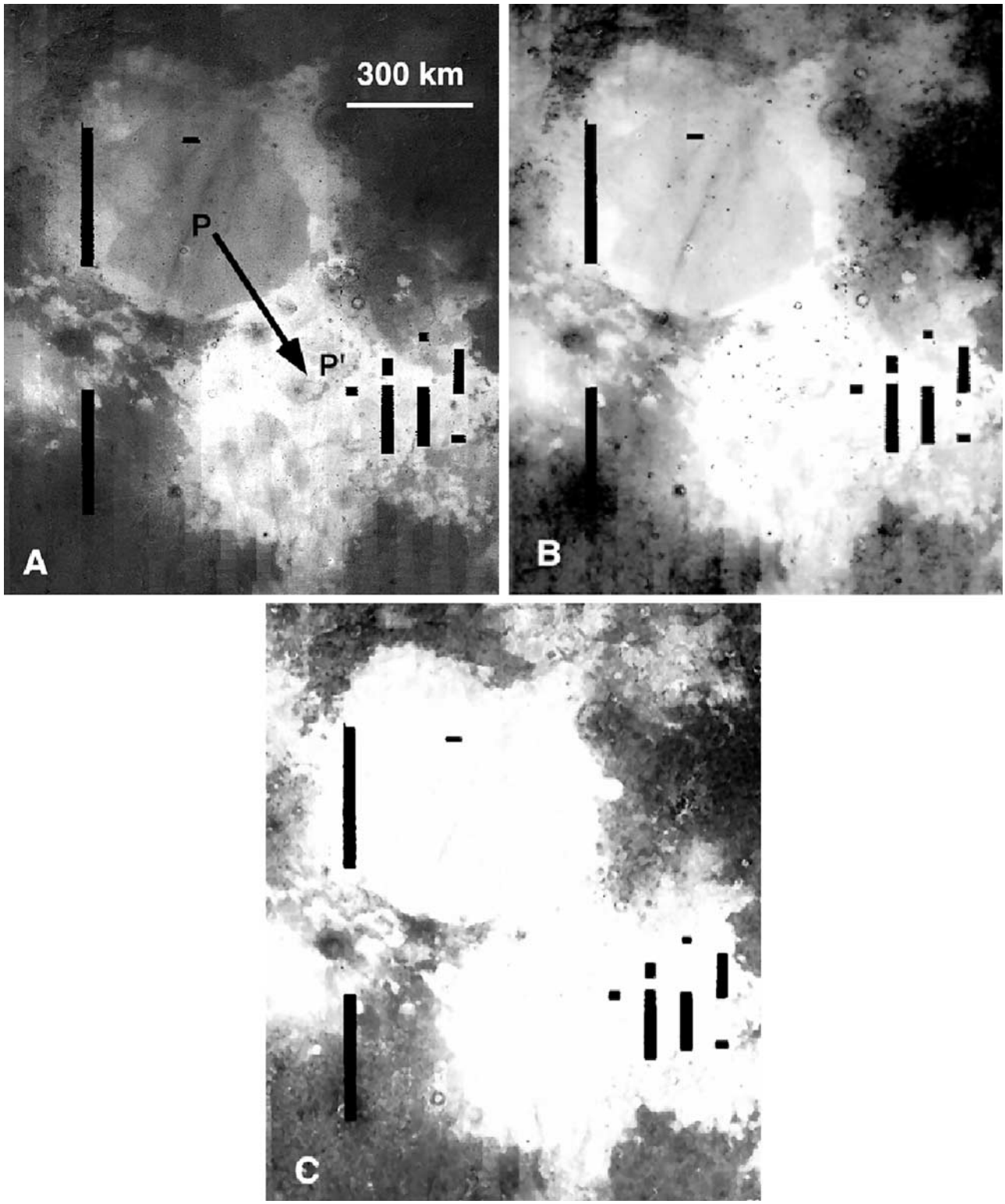

Figure 4. Results of spectral mapping along the boundary between Mare Serenitatis (red mare) and Mare Tranquillitatis (blue mare). (a) TiO_2 map, (b) mare fraction from traditional SMA, and (c) aggregated mare fraction from MESMA.

Tranquillitatis, and (2) along the mare-mare contact within Mare Humorum. These boundaries between low-and high-Ti mare units are very distinct in the TiO_2 maps (Figures 4a and 5a). Lateral mixing across these mare-mare boundaries should result in a compositional gradient between the mare units, but not a mare-highland gradient. A mare-highland material gradient would require introduction of significant highland materials by the mixing processes.

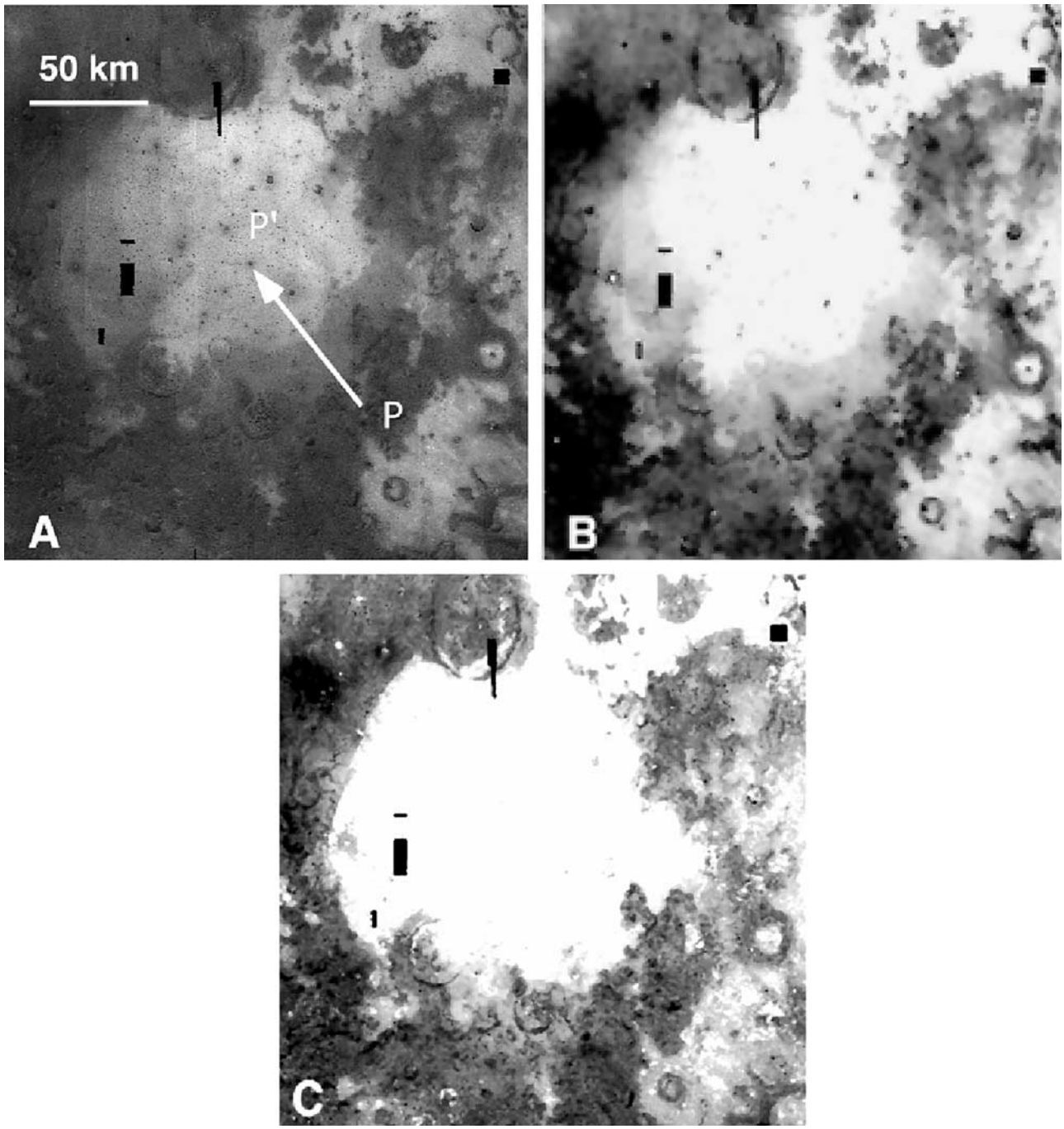

Figure 5. Results of spectral mapping of the mare-mare boundary within Mare Humorum. (a) TiO_2 map, (b) mare fraction from traditional SMA, and (c) aggregated mare fraction from MESMA.

[38] The compositional contrast between the low-Ti basalts in Mare Serenitatis and the high-Ti basalts in Mare Tranquillitatis have been well documented [e.g., *Johnson et al.*, 1991; *Melendrez et al.*, 1994; *Bell and Hawke*, 1995; *Staid et al.*, 1996; *Staid and Pieters*, 2000; *Li and Mustard*, 2001]. Compositionally distinct components consist of low-Ti and high-Ti mare, mature highland, fresh low-and high-Ti mare materials, fresh highland materials and dark mantling material at the Taurus-Littrow region and surrounding Mare Serenitatis. This suggests that at least seven end-members are required to describe compositions within this region.

[39] On the basis of near infrared reflectance and 70-cm radar data, pure anorthosite and noritic anorthosite highland rocks were identified at the northwest portion of the Humorum basin [*Hawke et al.*, 1993]. Four types of mare basalt, including low-and high-Ti content, with basaltic pyroclastic deposits were described by *Pieters et al.* [1975]. Fresh highland materials were excavated within Mare Humorum by large impacts [*Budney and Lucey*, 1998]. Combining these components with the mare basalts suggests that eight end-members would be required for a rigorous and complete mixture analysis. With only five-band Clementine

UVVIS data, SMA can't resolve all distinct components within both regions for the end-member fractions.

[40] The TiO_2 maps shown in Figures 4a and 5a demonstrate clear mare-mare boundaries in two areas. The correspondent mare fraction images in Figures 4b and 5b derived by traditional SMA also revealed the mare-mare boundaries. There is no doubt that traditional SMA casts the titanium difference of mare units in all three areas onto varying mare-highland fractions. In mare fraction images generated by MESMA Figures 4c and 5c, the mare-mare boundaries are not distinct, indicating its insensitivity to the variation in mare compositions.

[41] To further highlight the performance of MESMA over SMA, compositional profiles were drawn across these three mare-mare boundaries. Figures 6a and 6b show the variation of Ti content and the mare fraction by traditional SMA across the mare-mare boundaries between Serenitatis and Tranquillitatis and within Humorum mare. In Figure 6a, the range of TiO_2 content from 8.1% to 12.4% induces a variation of mare fractions from 75% to 85% for the SMA results. This is balanced by a 10% variation in highland abundance to accommodate the 4.3% TiO_2 difference between mare basalts. Similarly, a range of TiO_2 content from 4.1% to 6.3% induces a variation of mare abundance from 60% to 70% in Figure 6b. This is due to the fact that the absence of a low-Ti mare end-member causes its relative contribution to partition into the fractions of the other end-members. For the most part, this is partitioned into highland components, thus raising highland abundance. However, the MESMA profiles across three low- and high-Ti mare boundaries are flat as shown in Figures 6a and 6b. MESMA is insensitive to the variation in Ti content in a mixture context because it adjusts the end-members dynamically. There are however, discrete jumps in the MESMA profiles. These jumps represent locations where the pixels are poorly modeled by MESMA. The fractions of highland and mare for these pixels were set to zero in the MESMA fraction maps, and this resulted in some break points in the unsmoothed MESMA profiles. The discrete jumps originate from the break points of unsmoothed MESMA profiles after applying a filter procedure to clean the noise.

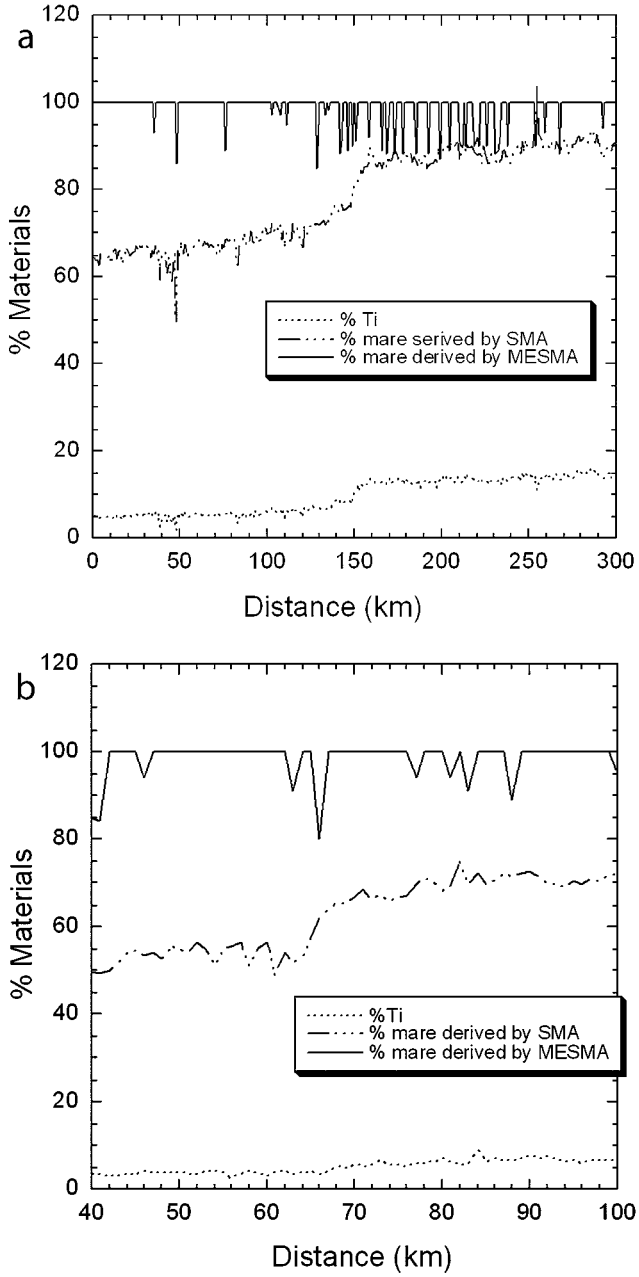

Figure 6. Smoothed profiles show the variation of TiO_2 content and mare fractions resulting from SMA and MESMA and across mare-mare boundaries (a) Mare Serenitatis and Mare Tranquillitatis, (b) Mare Humorum.

5. Highland Contamination of Mare Surfaces

[42] In this section, we will use the MESMA highland fraction image to assess lateral mixing of highland on mare surfaces in three basins Nectaris, Fecunditatis and Crisium.

5.1. Mare Nectaris

[43] Nectaris is a multiring basin, 860 km in diameter, centered at 16°S, 34°E [*Whitford-Stark*, 1981; *Wilhelms*, 1987]. Mare Nectaris, bounded by a 400 km ring, occupies about 84,000 km^2 of the central portion of the Nectaris basin [*Whitford-Stark*, 1981]. The mineral compositions are similar to those from the Apollo 12 site [*Pieters*, 1978; *Whitford-Stark*, 1981]. The age of these mare basalts was estimated to be between 3.5 to 3.75 b.y., while the earliest basalts can be as old as 3.79 b.y. [*Whitford-Stark*, 1981]. The diagram of these mare basalt deposits is shown in Figure 7.

[44] Impact cratering was one of the most important factors shaping the Nectaris basin in its post-mare history. A distinctive feature is the large highland crater Theophilus, a 100-km diameter Eratosthenian crater lying between the second and third Nectaris rings as shown in Figure 7 [*Wilhelms*, 1987]. Theophilus' rays are separated from their crater in northern Tranquillitatis by a distance of 600 km. The rays were identified as major sources of highland contamination at the Apollo 11 landing site [*Staid et al.*, 1996]. Theophilus has a larger diameter than any other craters in the Mare Nectaris region, suggesting that it played the most important role in lateral mixing of highland material into Mare Nectaris. The 25-km diameter crater Mädler lies on Theophilus ejecta, but the crater interior contains 70–80% highland material, suggesting the Mädler

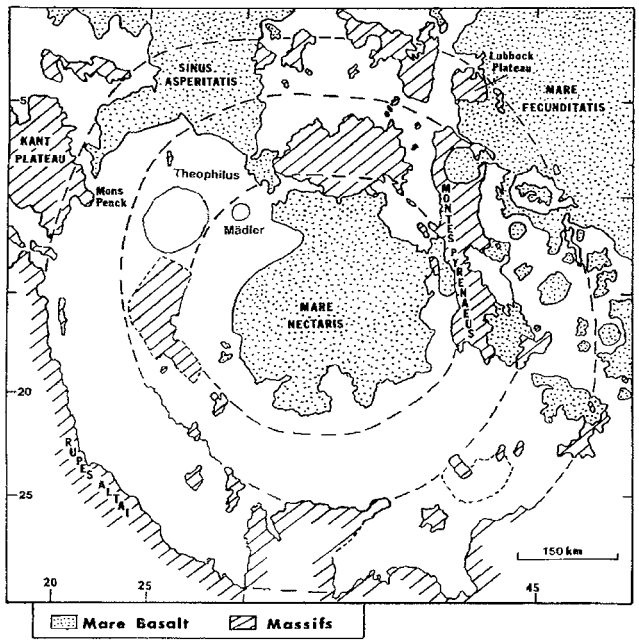

Figure 7. Schematic geological map of Nectaris basin. The dashed lines indicate the ring system. (Reprinted from *Whitford-Stark* [1981] with permission from Elsevier.)

impact excavated little mare, and to a large extent redistributed the highland ejecta over the mare.

[45] To assess the amount of highland introduced by Theophilus' rays into the mare surface, profiles were extracted from the aggregated MESMA highland fraction image at the locations shown in Figure 8. The profiles are shown in Figure 9. The first three profiles, P1, P2 and P3 in Figure 9a demonstrate the variation of highland concentration across the mare and perpendicular to the ballistic ejecta emplacement at increasing radial distances from Theophilus with each additional profile. For the mare-highland boundary, they all exhibit a relatively symmetric profile and a transition from highland to mare, a typical trend reflecting

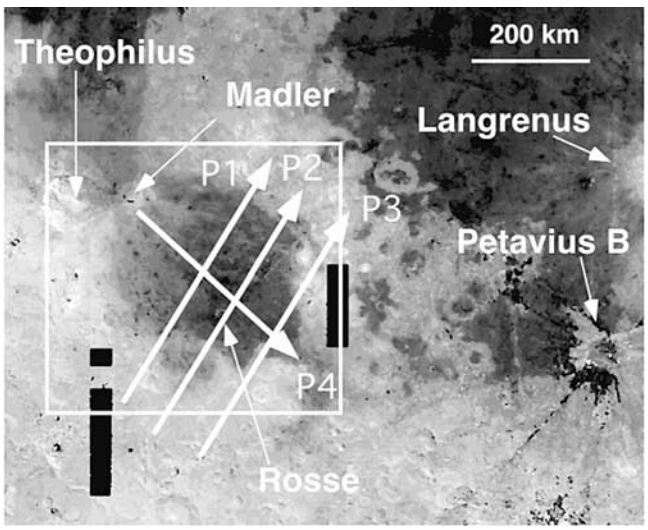

Figure 8. Profiles locations and large craters surrounding Mare Nectaris are shown with Highland fraction images of MESMA.

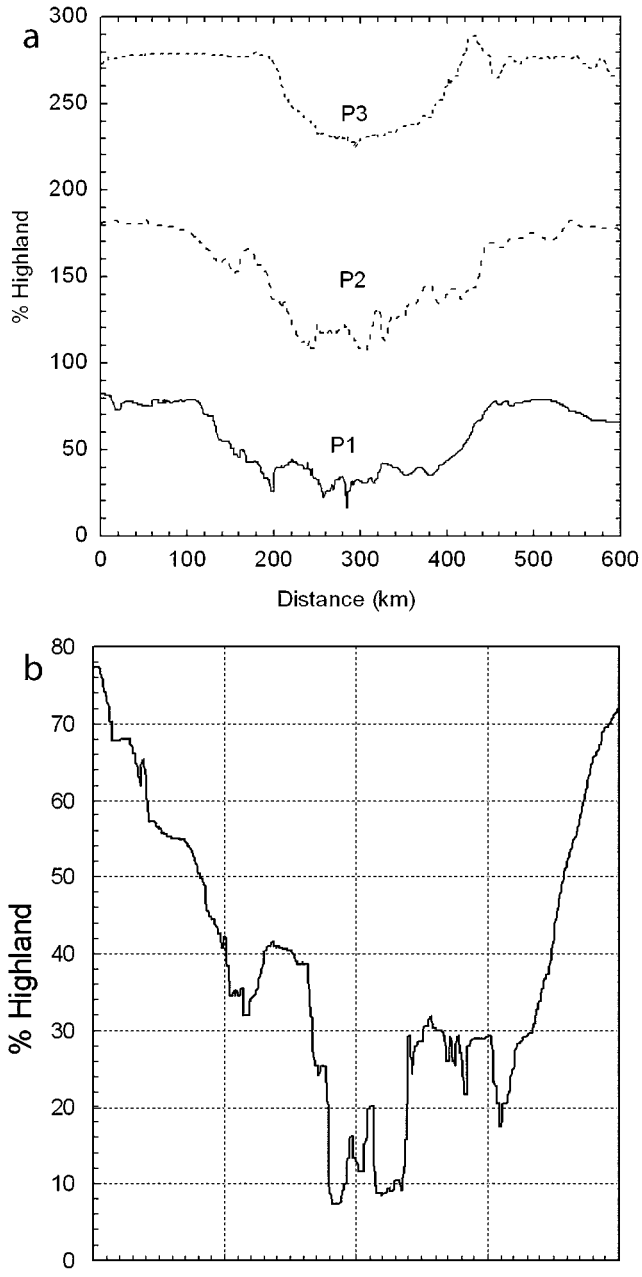

Figure 9. Profiles across Mare Nectaris show the variation of highland abundances. (a) Across radial direction of Theophilus (Mädler) ejecta (P1–P3),%100 shift in vertical axis for clarity; and (b) along the radial direction (P4).

lateral mixing due to small impacts [*Li and Mustard*, 2000]. In contrast, the fourth profile, P4 in Figure 9b, is highly asymmetric and reflects the continuous variation of highland abundance with respect to Theophilus and Mädler impacts. The extent of highland contamination is as high as 70–80% close to Mädler in northwestern Mare Nectaris, but as low as 20–30% in the southeastern part of the Mare Nectaris, furthest from the Theophilius crater.

5.2. Mare Fecunditatis

[46] Fecunditatis is a pre-Nectarian irregular basin, 600 km by 900 km across, filled with middle to late late-Imbrian

aged mare basalt [*Dehon and Waskom*, 1976; *Wilhelms*, 1987]. Mare basalt covers an area of approximately 220,000 km^2 and is elongated in a north-south direction [*Whitford-Stark*, 1986]. Samples returned with Luna 16 were typically high iron, high alumina basalt with a radiometric age of 3.41 b.y. [*Wilhelms*, 1987].

[47] *Li and Mustard* [2000] interpreted a symmetric compositional boundary across the mare-highland contact in Northern Mare Fecunditatis as a compositional gradients resulting from lateral mixing due to repetitive small impacts. The two largest post-mare impacts surrounding Mare Fecunditatis are Taruntius and Langrenus. Taruntius, a Copernican aged crater, has a diameter of 56 km and Langrenus, an Eratosthenian-aged crater, is 132 km across [*Wilhelms*, 1987]. The continuous ejecta and crater rays from both impacts caused lateral mixing of highland with mare materials over a significant portion of Mare Fecunditatis.

[48] The highland fraction image of Mare Fecunditatis (Figure 10) shows the contamination by highland ejecta from the craters Taruntius and Langrenus. An end-to-end profile of highland abundance across Mare Fecunditatis (Figure 11) was extracted along the location shown in Figure 10. The highland abundance gradually decreases with increasing radial distance from Taruntius, to a minimum of 5% at 175 km from the crater. From there, the abundance increases rapidly to 20% over another 130 km and then increases more gradually to 40% in the next 190 km near the Langrenus rim. Between 370 and 390 km from Taruntius, two troughs of relatively pure mare were excavated from the beneath regions of abundant highland material by dark halo craters. The v-shaped gradient pattern revealed by the profiles indicates that lateral mixing by Taruntius and Langenus was dominant over vertical mixing of highland into the mare.

[49] These results are in contrast with the detailed analyses by *Farrand* [1988]. *Farrand* [1988] concluded that highland contamination in Mare Fecunditatis was due to vertical mixing rather than lateral mixing. He based his conclusion on an isopach map of basalt thicknesses (Figure 12a) and highland contamination maps derived from an ''inverse mixing model'' of geochemical elements (Figure 12b) [*Farrand*, 1988]. He found that an east-west trending swath with low highland abundance on the contamination maps was well correlated to the trend of the thickest mare from the isopach map (Figure 12a), implying an efficient vertical mixing. He argued that if lateral mixing were dominant, the lowest highland contamination levels would occur at a point equidistant from the surrounding highland and follow an elongated north-south trend.

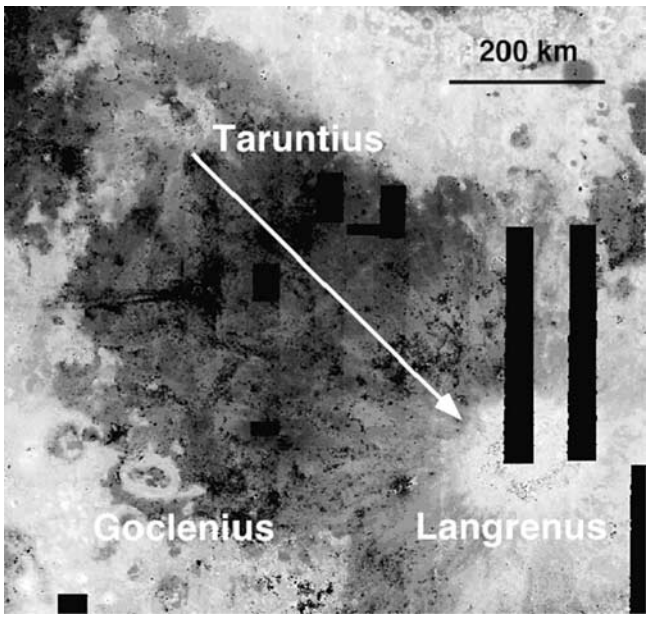

Figure 10. Highland fraction image of Mare Fecunditatis resulting from MESMA. The line with arrow shows the direction and location of the profile shown in Figure 11.

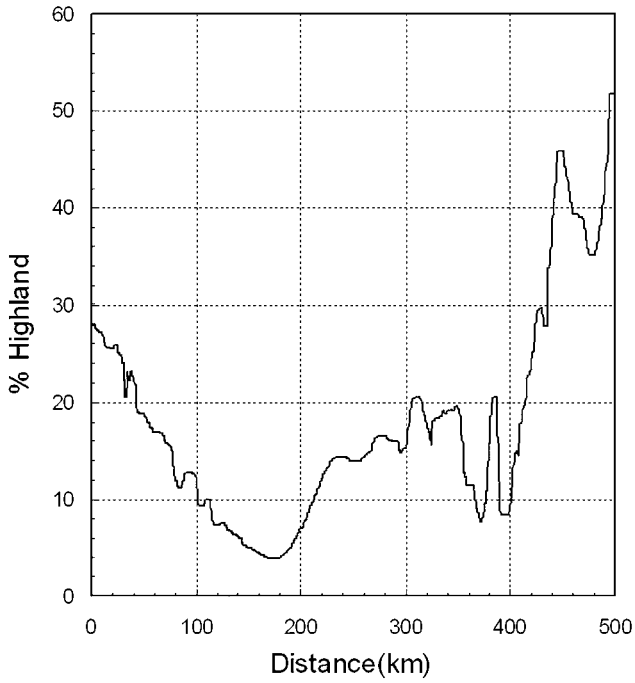

Figure 11. Variation of highland abundances across Mare Fecunditatis.

[50] We tested this hypothesis by isolating pixels shown in Figure 10 with highland abundances between 1% and 15%, shown in Figure 13. In Figure 13, there is a northeast-southwest trend approximately perpendicular to the profile direction shown Figure 10. In the northeastern Mare Fecunditatis, there is a distinct low highland contamination region correlated with basalt spectrally characterized by medium-high UV/VIS ratios, dark albedo, weak 1 μm band absorption and the absence of 2 μm band absorption [*Pieters*, 1978]. The specific distribution of low highland abundances in Figure 13 is not consistent with the trend of highland contamination shown in Farrand's isopach maps, Figure 12b. Our observations indicate that there is no apparent correlation of highland contamination with mare basalt thickness. This observation strongly argues that lateral mixing due to Taruntius and Langrenus is responsible for the highland contamination into Mare Fecunditatis, while vertical mixing is insignificant.

5.3. Mare Crisium

[51] Crisium is a multiring basin with an age between Nectaris and Imbrium [*Wilhelms*, 1987]. The diameters of

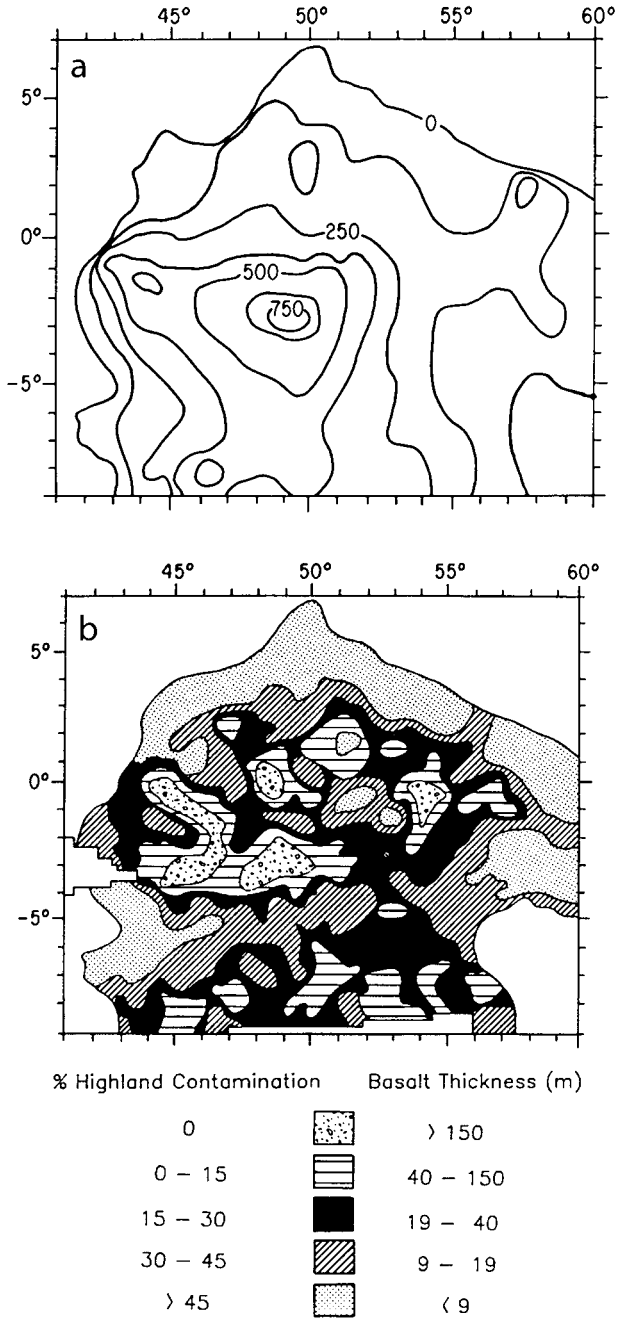

Figure 12. Isopach of basalt thickness in meters (a) and highland contamination (b) maps of the northern Mare Fecunditatis [after *Farrand*, 1988]. (Reprinted with permission of Lunar and Planetary Institute, Houston, Texas.)

its three rings are estimated to be 540, 740 and 1060 km [*Wilhelms*, 1987; *Bussey and Spudis*, 2000], but the rim diameter is controversial [*Wilhelms*, 1987]. Mare basalt filled in an elliptical region, 420 km North-South by 560 km East-West, approximately 188,500 km^2 [*Wilhelms*, 1987]. Mare Crisium has been divided into three spectral units on the basis of multispectral images and telescopic reflectance spectra [*Adams et al.*, 1978; *Head et al.*, 1978; *Pieters et al.*, 1979]. The map of spectral classification in Figure 14a and unit nomenclature in Figure 14b are after *Head et al.* [1978]. Group I represents Fe-Mg rich titaniferous basalt similar to Luna 16 samples, Group II is very low-Ti and feldspathic ferrobasalt similar to Luna 24 samples, and Group III refers to low-Ti ferrobasalt similar to samples from Apollo 12.

[52] Post-mare craters in the surrounding highland created the observed ray systems in Mare Crisium, with distinct bright clear-cut boundaries. Investigation of the rays in Crisium indicates that some include primary highland ejecta from the source craters [*Maxwell and El-Baz*, 1978]. The rays from the crater Proclus are the most distinct in the highland fraction image (Figure 15). At least five rays from this crater can be found within Mare Crisium and reached the group II mare unit. The rays from other craters are mostly overlain by Proclus ejecta.

[53] Highland contamination of Mare Crisium (Figure 15) is higher in the northwestern and eastern parts of the basin. Highland contamination in the northwest primarily results from Proclus, a Copernican-aged crater, approximately 28 km in diameter, with an asymmetric bright ray system. This part of Mare Crisium is located down range of the crater ejecta and three distinct rays are observed in this area. A great deal of highland ejecta from Proclus is present in this region. A set of rays from an unspecified source north of Crisium is observed to interleave with those of Proclus. This contamination is evident in Figure 15 where pixels having a highland abundance between 1 to 50% are shown. Overlapping of these rays resulted in a large amount of highland contamination (20–30%). A comparison of Figure 14a and Figure 15 indicates that this area of highland contaminated is correlated with group II mare plus the spectrally undivided region. The group III mare is located in an area with less highland contamination, less than 20% in west and south-east areas. Therefore some basalt classification in this region may reflect highland contamination of the spectral properties.

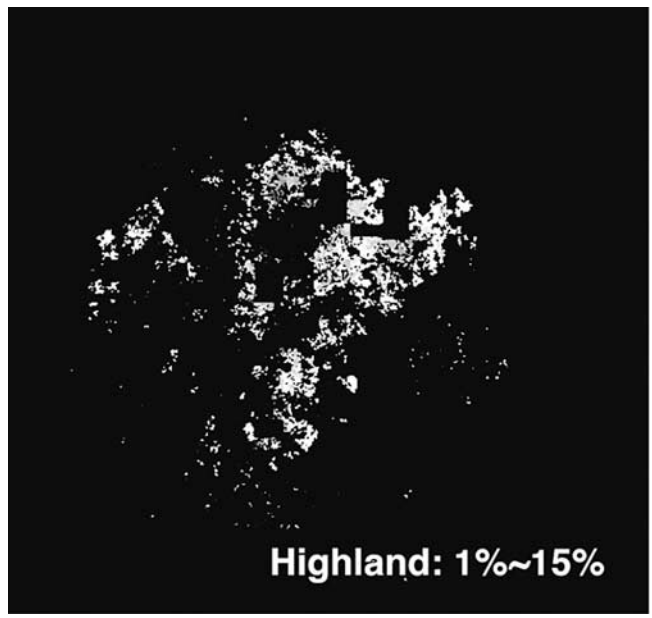

Figure 13. Highland contamination map derived from MESMA. Only pixels with <15% highland abundance are plotted.

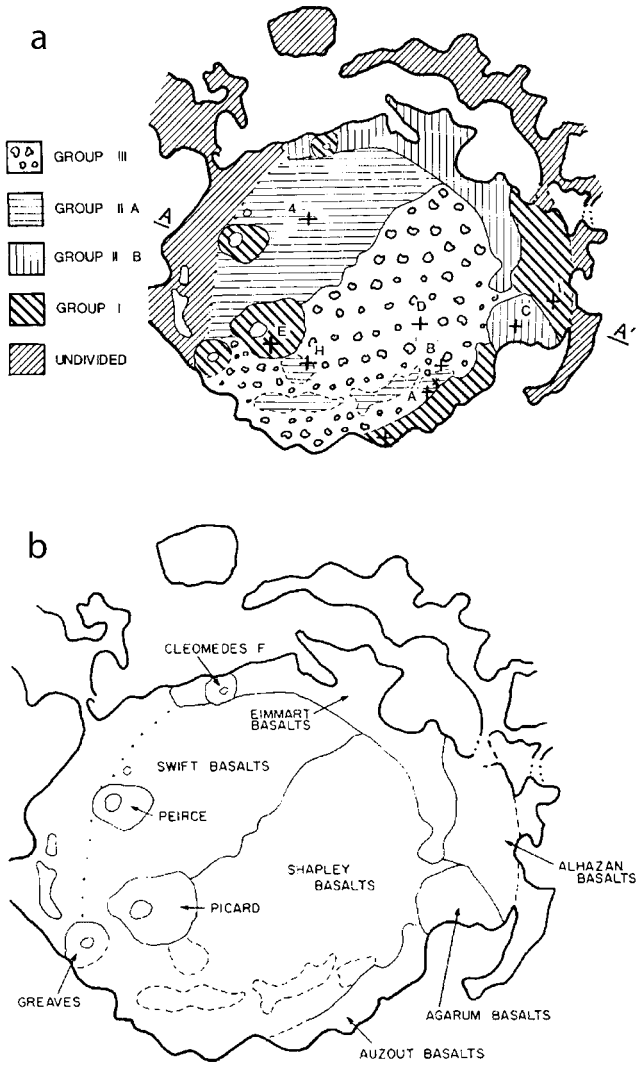

Figure 14. Schematic geological maps of Mare Crisium. (a) Compositional units and (b) unit nomenclature. (Reprinted with permission from *Head et al.* [1978].)

[54] The eastern Mare Crisium, area contains a large amount of highland contamination in two mare basalts: Alahzan and Argarum (Figure 15). We attribute the highland contamination in the Alahzan region to the ejecta from the Hansen and Condorcet T craters. Hansen is an Upper Imbrian-aged crater, the same age as the Crisium mare [*Wilhelms*, 1987]. Because of its medium size, a 12-km diameter, and proximity to Crisium, it is the source of a large amount of highland ejecta in the mare. As shown in Figure 15, Condorcet T is a Copernican-aged crater exhibiting a bright north-northwest ray system that obscures much of Argarum type basalt [*Maxwell and El-Baz*, 1978]. The Agarum basalts were described as LBSP due to low-FeO and TiO_2 content [*Pieters*, 1978; *Head et al.*, 1978; *Wilhelms*, 1987]. The meaning of letters in the type designation is: L, low UV/VIS ratio; B, bright in albedo; S, strong 1 μm band absorption; and P, 2.0 μm absorption is present. We believe that a very asymmetric ejecta pattern of Condorcet T must also affect the Alahzan basalt. If so, it contributed to the highland contamination shown in Figure 15.

[55] The northern edge of Mare Crisium, in Figure 15, also shows a large highland contamination in the Emmart basalt classified as LBSP [*Wilhelms*, 1987]. We believe that highland contamination is a significant component of the spectral characteristics of LBSP, and the LBSP signatures of mare basalt in these areas are not inherent.

6. Conclusion

[56] Multiple end-member spectral mixture analysis (MESMA) was applied to Clementine UVVIS global mosaic data to map lunar surface compositions. Unlike traditional spectral mixture analysis (SMA) using a fixed end-member set, MESMA decomposes each pixel spectrum with an optimal end-member set and allows for adjusting end-members combinations dynamically. As such, MESMA allows for the application of a 13-end-member set to the decomposition of the Clementine UV-VIS 5-band data. Comparing the results from spectral mixture analysis (SMA) for Serenitatis/Tranquillitatis boundary with those from MESMA suggests that MESMA can accommodate the compositional variation of mare components, and provides more accurate estimates of highland contamination. Similar comparisons were obtained in the Mare Humorum.

[57] Using estimated highland material content, we investigated relics of highland material dispersion and assessed the extent of highland contamination in Mare Nectaris, Mare Fecunditatis, and Mare Crisium due to the proximal large craters, Theophilus, Taruntius, Langrenus, and Proclus. Highland fraction images show that highland abundances are still significant at sites several radii distant from these large craters. The analyses of the compositional gradient profiles, extending several hundred kilometers, indicated that Theophilus impact resulted in highland contamination of 20–80% on most of Mare Nectaris while Taruntius and Langrenus impacts caused 5–40% contamination of Mare Fecunditatis. The trend of minimal highland

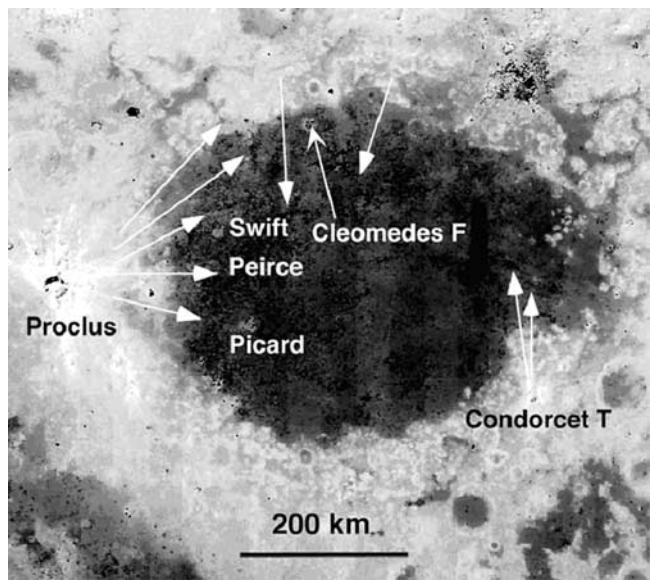

Figure 15. Highland fraction images of Mare Crisium resulting from MESMA. Craters are labeled and white arrows indicate crater rays.

abundance in Mare Fecunditatis correlates poorly with basalt thickness, suggesting an insignificant vertical mixing. Proclus, combining with other craters, was responsible for highland contamination in most of Mare Crisium surface. A large highland contamination is found in some LBSP basalts of Mare Crisium. We believe that highland contamination is a significant component of the spectral characteristics of LBSP, and the LBSP signatures of mare basalt in these areas are not inherent. The results from this study support that large impacts played a dominant role in delivering highland materials on three mare surfaces.

[58] **Acknowledgments.** The authors are grateful for numerous helpful comments of two referees, L. R. Gaddis and P. G. Lucey, whose contributions significantly improved the quality of the manuscript. We would like to thank M. L. Whiting and S. Tompkins for their comments and generous help. We also acknowledge the assistance of Peter Neivert, Bill Fripp and Ma Xia for their technical support. Partial support from the NASA Lunar Data Analysis and Planetary Geology and Geophysics programs is gratefully acknowledged.

References

Adams, J. B., J. W. Head, T. B. McCord, C. M. Pieters, and S. Zisk, Mare Crisium: Regional stratigraphy and geologic history, *Geophys. Res. Lett.*, *5*, 313–316, 1978.

Bell, J. F., and B. R. Hawke, Compositional variability of the Serenitatis/Tranquillitatis region of the Moon from telescopic multispectral imaging and spectroscopy, *Icarus*, *118*, 51–68, 1995.

Budney, C. J., and P. G. Lucey, Basalt thickness in Mare Humorum: The crater excavation method, *J. Geophys. Res.*, *103*, 16,885–16,870, 1998.

Bussey, D. B. J., and P. D. Spudis, Compositional studies of the Orientale, Humorum, Nectaris and Crisium lunar basins, *J. Geophys. Res.*, *105*, 4235–4243, 2000.

Charette, M. P., T. B. McCord, C. M. Pieters, and J. B. Adams, Application of remote sensing spectral reflectance measurements to lunar geology classification and determination of titanium content of lunar soils, *J. Geophys. Res.*, *79*, 1605–1613, 1974.

Dehon, R. A., and J. D. Waskom, Geologic structure of the eastern mare basins, *Proc. Lunar Sci. Conf. 7th*, 2279–2746, 1976.

Eliason, E. M., et al., Digital processing for a global multispectral map of the Moon from Clementine UVVIS imaging instrument, *Lunar Planet. Sci.* [CD-ROM], *XXX*, abstract 1933, 1999.

Farrand, W. H., Highland contamination and minimum basalt thickness in northern Mare Fecunditatis, *Proc. Lunar Planet. Sci. Conf. 18th*, 319–329, 1988.

Florenskiy, K. P., A. T. Bazilevskiy, and A. V. Ivanov, The role of exogenic factors in the formation of the lunar surface, in *Proceedings of the Soviet-American Conference on Cosmochemistry of the Moon and Planets*, edited by J. H. Pomerov and N. H. Hubbard, pp. 571–584, NASA, Washington, D. C., 1974.

Gaddis, L. R., C. M. Pieters, and B. R. Hawke, Remote sensing of lunar pyroclastic mantling deposits, *Icarus*, *61*, 461–489, 1985.

Gaddis, L. R., B. R. Hawke, M. Robinson, and C. Coombs, Compositional analysis of small lunar pyroclastic deposits using Clementine multispectral data, *J. Geophys. Res.*, *105*, 4245–4262, 2000.

Gault, D. E., F. Horz, D. E. Brownlee, and J. B. Hartung, Mixing of the lunar regolith, *Proc. Lunar. Sci. Conf. 5th*, 2365–2386, 1974.

Giguere, T., G. J. Talor, B. R. Hawke, and P. G. Lucey, The titanium contents of lunar mare basalts, *Meteorit. Planet. Sci.*, *35*, 193–200, 2000.

Greeley, R., et al., Galileo imaging observations of lunar maria and related deposits, *J. Geophys. Res.*, *98*, 17,183–17,205, 1993.

Hapke, B., Bidirectional reflectance spectroscopy, 1, Theory, *J. Geophys. Res.*, *86*, 3039–3054, 1981.

Hapke, B., *Theory of Reflectance and Emittance Spectroscopy*, Cambridge Univ. Press, New York, 1993.

Hawke, B. R., et al., Remote sensing studies of the terrain northwest of Humorum basin, *Geophys. Res. Lett.*, *20*, 419–422, 1993.

Head, J. W., Lunar dark-mantle deposits: Possible clues to the distribution of early mare deposits, *Proc. Lunar Sci. Conf. 5th*, 207–222, 1974.

Head, J. W., J. B. Adams, T. B. McCord, C. M. Pieters, and S. Zisk, Regional stratigraphy and geologic history of Mare Crisium, in *Mare Crisium: The View From Luna 24*, edited by R. B. Merrill and J. J. Papike, pp. 43–74, Pergamon, New York, 1978.

Hörz, F., How thick are mare basalts?, *Proc. Lunar Planet. Sci. Conf. 9th*, 3311–3331, 1978.

Hörz, F., R. Grieve, G. Heiken, S. Spudis, and A. Binder, Lunar surface processes, in *Lunar Sourcebook*, pp. 61–120, Cambridge Univ. Press, New York, 1991.

Isbell, C. E., et al., Clementine: A multispectral digital image model archive of the Moon, *Lunar Planet. Sci.* [CD-ROM], *XXX*, abstract 1812, 1999.

Johnson, J. J., S. M. Larson, and R. Singer, Remote sensing of potential lunar resources: 1. Near-side compositional properties, *J. Geophys. Res.*, *96*, 18,861–18,882, 1991.

Johnson, T. V., R. S. Saunders, D. L. Matson, and J. A. Mosher, A TiO_2 abundance map for the northern maria, *Proc. Lunar Sci. Conf. 8th*, 1029–1036, 1977.

Li, L., and J. F. Mustard, Compositional gradients across mare-highland contacts: The importance of lateral mixing and geological implications, *J. Geophys. Res.*, *105*, 20,431–20,450, 2000.

Li, L., and J. F. Mustard, Improved mapping of the lunar surface using a multiple endmember mixture model, *Lunar Planet. Sci.* [CD-ROM], *XXXII*, abstract 2052, 2001.

Lucey, P. G., D. T. Blewett, and B. R. Hawke, Mapping the FeO and TiO_2 content of the lunar surface with multispectral imagery, *J. Geophys. Res.*, *103*, 3679–3699, 1998.

Lucey, P. L., D. T. Blewett, and B. L. Jolliff, Lunar iron and titanium abundance algorithm based on final processing of Clementine ultraviolet-visible images, *J. Geophys. Res.*, *105*, 20,297–20,305, 2000a.

Lucey, P. L., D. T. Blewett, G. J. Taylor, and B. R. Hawke, Imaging of lunar surface maturity, *J. Geophys. Res.*, *105*, 20,377–20,386, 2000b.

Maxwell, T. A., and F. El-Baz, The nature of rays and sources of highland material in Mare Crisium, in *Mare Crisium: The View From Luna 24*, edited by R. B. Merrill and J. J. Papike, pp. 89–103, Pergamon, New York, 1978.

McEwen, A. S., E. Elison, P. Lucey, E. Malaret, C. Pieters, M. Robinson, and T. Sucharski, Summary of radiometric calibration and photometric normalization steps for the Clementine UVVIS images, *Lunar Planet. Sci.* [CD-ROM], *XXIX*, abstract 1466, 1998.

Melendrez, D. J. J., S. M. Larson, and R. B. Singer, Remote sensing of potential lunar resources: 2. High spatial resolution mapping of spectral reflectance ratios and implications for nearside mare TiO_2 contents, *J. Geophys. Res.*, *99*, 5601–5619, 1994.

Mustard, J. F., and C. M. Pieters, Quantitative abundance estimates from bidirectional reflectance measurements, *Proc. Lunar Planet. Sci. Conf. 17th*, Part 2, *J. Geophys. Res.*, *92*, suppl., E617–E626, 1987.

Mustard, J. F., and C. M. Pieters, Photometric phase functions of common geologic minerals and applications to quantitative analysis of mineral mixture reflectance spectra, *J. Geophys. Res.*, *94*, 13,619–13,634, 1989.

Mustard, J. F., L. Li, and G. He, Nonlinear spectral mixture modeling of lunar multispectral data: Implications for lateral transport, *J. Geophys. Res.*, *103*, 19,419–19,425, 1998.

Oberbeck, V. R., R. H. Morrison, F. Hörz, W. L. Quaide, and D. E. Gault, Smooth plains and continuous deposits of craters and basins, *Proc. Lunar Sci. Conf. 5th*, 111–136, 1974.

Oberbeck, V. R., F. Hörz, R. H. Morrison, W. L. Quaide, and D. E. Gault, On the origin of the lunar smooth plains, *Moon*, *12*, 19–54, 1975.

Pieters, C. M., Characterization of lunar mare basalt types-II: Spectral classification of fresh mare craters, *Proc. Lunar Sci. Conf. 8th*, 1037–1048, 1977.

Pieters, C. M., Mare basalt types on the front side of the Moon: A summary of spectral reflectance data, *Proc. Lunar Planet. Sci. Conf. 9th*, 1978–2849, 1978.

Pieters, C. M., and T. B. McCord, Characterization of lunar basalt types: I. A remote sensing study using reflectance spectroscopy of surface soils, *Proc. Lunar Sci. Conf. 7th*, 2677–2690, 1976.

Pieters, C. M., and S. Tompkins, Tsiolkovsky craters: A window into crustal processes on the lunar farside, *J. Geophys. Res.*, *104*, 21,935–21,949, 1999.

Pieters, C., J. W. Head, T. B. McCord, J. B. Adams, and S. Zisk, Geochemical and geological units of Mare Humorum: Definition using remote sensing and lunar sample information, *Proc. Lunar Sci. Conf. 6th*, 2689–2710, 1975.

Pieters, C. M., T. B. McCord, J. W. Head, J. B. Adams, and S. Zisk, Mare Crisium geologic units: Implications of additional remote sensing data, *Proc. Lunar Planet. Sci. Conf. 10th*, 2967–2973, 1979.

Pieters, C. M., J. M. Head, J. B. Adams, T. B. McCord, S. H. Zisk, and Whitford-Stark, Late high titanium basalt of the western maria: Geology of the Flamsteed region of Oceanus Procellarum, *J. Geophys. Res.*, *85*, 3913–3938, 1980.

Pieters, C. M., J. B. Adams, P. Mouginis-Mark, S. H. Zisk, M. O. Smith, and J. W. Head, The nature of crater rays: The Copernicus example, *J. Geophys. Res.*, *90*, 12,393–12,413, 1985.

Pieters, C. M., et al., Crustal diversity of the Moon: Compositional analysis of Galileo SSI data, *J. Geophys. Res.*, *98*, 17,127–17,148, 1993.

Pieters, C. M., M. I. Staid, E. M. Fisher, S. Tompkins, and G. He, A sharp view of impact craters from Clementine data, *Science*, *266*, 1844–1848, 1994.

Pieters, C. M., S. Tompkins, J. W. Head, and P. C. Hess, Mineralogy of the Mafic anomaly in the South Pole-Aitken basins: Implications for excavation of the lunar mantle, *Geophys. Res. Lett.*, *24*, 1903–1906, 1997.

Pieters, C. M., J. W. Head, L. Gaddis, B. Jolliff, and M. Duke, The character and possible origin of olivine in South Pole-Aitken basin, *Lunar Planet. Sci.* [CD-ROM], *XXXII*, abstract 1810, 2001.

Quaide, W. L., and V. Oberbeck, Development of the mare regolith: Some model considerations, *Moon*, *13*, 27–55, 1975.

Rhodes, J. M., Some compositional aspects of lunar regolith evolution, *Philos. Trans. R. Soc. London, Ser. A*, *285*, 293–301, 1977.

Roberts, D. A., M. Gardner, R. Church, S. Ustin, G. Scheer, and R. O. Green, Mapping Chaparral in the Santa Monica Mountains using multiple endmember spectral mixture models, *Remote Sens. Environ.*, *65*, 267–279, 1998.

Robinson, M. S., A. S. McEwen, E. Elison, M. E. M. Lee, E. Malaret, and P. G. Lucey, Clementine UVVIS global mosaic: A new tool for understanding the lunar crust, *Lunar Planet. Sci.* [CD-ROM], *XXX*, abstract 1931, 1999.

Schultz, P. H., and D. E. Gault, High-velocity clustered impacts: Experimental results, *Lunar Planet. Sci.*, *XVI*, 674–675, 1983.

Schultz, P. H., and D. E. Gault, Clustered impacts: Experiments and implications, *J. Geophys. Res.*, *90*, 3701–3732, 1985.

Staid, M. I., and C. M. Pieters, Integrated spectral analysis of mare soils and craters: Application to eastern nearside basalt, *Icarus*, *145*, 122–139, 2000.

Staid, M. I., C. M. Pieters, and J. W. Head, Mare Tranquillitatis: Basalt emplacement history and relation to lunar samples, *J. Geophys. Res.*, *101*, 23,213–23,228, 1996.

Stöffler, D., H. D. Knoll, U. B. Marvin, C. H. Simon, and P. H. Warren, Recommended classification and nomenclature of lunar highland rocks-a committee report, in *Proceedings of the Conference on the Lunar Highlands Crust*, edited by J. J. Papike and R. B. Merill, pp. 71–70, Pergamon, New York, 1980.

Tompkins, S., and C. M. Pieters, Mineralogy of the lunar crust: Results from Clementine, *Meteorit. Planet. Sci.*, *34*, 25–41, 1999.

Weitz, C. A., J. W. Head, and C. M. Pieters, Lunar regional dark mantle deposits: Geological multiple spectral, and modeling studies, *J. Geophys. Res.*, *103*, 22,725–22,759, 1998.

Whitford-Stark, J. L., The evolution of the lunar Nectaris multiring basin, *Icarus*, *48*, 393–427, 1981.

Whitford-Stark, J. L., The geology of the lunar mare Fecunditatis (abstract), *Lunar Planet. Sci.*, *XVII*, 940–941, 1986.

Wilhelms, D. E., *The Geological History of the Moon*, *U.S. Geol. Surv. Prof. Pap.*, *1348*, 245 pp., 1987.

Yingst, R. A., and J. W. Head, Geology of mare deposits in South Pole-Aitken basin as seen by Clementine UV/VIS data, *J. Geophys. Res.*, *104*, 18,957–18,979, 1999.

Zisk, S. H., C. A. Hodges, H. J. Moore, R. W. Shorthill, T. W. Tompson, E. A. Whitaker, and D. E. Wilhelms, The Aristarchus-Harbinger region of the Moon: Surface geology and history from recent remote-sensing observations, *Moon*, *17*, 59–99, 1977.

L. Li, Center for Spatial Technologies and Remote Sensing, Department of Land, Air and Water Resources, University of California, One Shields Avenue, Davis, CA 95616, USA. (li@cstars.ucdavis.edu)

J. F. Mustard, Department of Geological Sciences, Box 1846, Brown University, Providence, RI 02906, USA.